ISBN: 978-3-95450-214-1 ISSN: 2673-5490 doi:10.18429/JACoW-IPAC2021-THPAB063

LASER TRANSPORT SYSTEM OF SHANGHAI LASER ELECTRON GAMMA SOURCE (SLEGS)*

H. H. Xu†, G. T. Fan
Shanghai Advanced Research Institute, Chinese Academy of Sciences, Shanghai, China

Abstract

Shanghai Laser Electron Gamma Source (SLEGS) [1], based on laser Compton scattering (LCS), as one of beamlines of Shanghai Synchrotron Radiation Facility (SSRF) in phase II, is under construction now. The technical design of its laser injection system has been implemented and optimized consecutively over the last few years.

In order to inject the 10640 nm CO_2 laser into the interaction point from the laser hutch outside the storage ring's shielding, a laser transport system longer than 20 m using relay-imaging telescopes is designed. There are two operation mode in SLEGS. One is backscattering mode, which will make the laser and electron bunch collide at 180º with flux higher than 10^7 γ/s. The other mode is slanting mode, which mainly inherits the design used in the prototype [2].

In this paper, a brief summary of the laser transport system is given. The system contains several modules to perform beam expansion, combining, monitoring and real-time adjustment. The design models, simulation study of the laser quality through the transportation, and the experimental results are presented.

INTRODUCTION

The RMS transverse beam size of electron bunch inside SSRF is 296.6 μm in horizontal and 13.26 μm in vertical at the colliding point, and the laser waist size would be focused to about 100 μm in slanting mode (S mode) and about 1.5 mm in backscattering mode (B mode) respectively according to the physical design, and the misalignment would result in the drop of gamma production. So a stable, adjustable and observable laser transport system is required. The overall layout of the laser transport system is showed in Fig. 1. It mainly include five parts: combination module, intermediate mirror groups and windows, adjustment module, detection module, and control module.

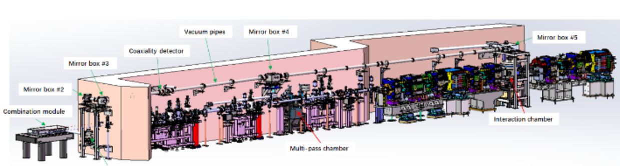

Figure 1: Laser transport system's layout over the frontend facilities and magnet lattice.

* Work supported by National Natural Science Foundation of China (No. 11405247, No.11875311, No. 11905274, No. 12005280)
†xuhanghua@zjlab.org.cn

Intermediate Mirror Groups and Windows

This part of the laser transport system is for turning and climbing the light path according to the on-site environment. Most of the mirrors are installed in a low-vacuum pipeline to reduce the attenuation of CO_2 laser energy caused by air absorption and the jitter caused by airflow. Except for ZnSe windows, all the optical components are reflective to reduce dispersion effect. A pair of off-axis parabolic mirrors is included to constrain the divergence of Gaussian beams in the long distance transmission.

KEY MODULES

Intermediate mirror groups and windows are not enough for the features we want, so the combination, adjustment and detection modules are added.

Combination Module

Since 10.6 μm CO_2 laser is invisible, we use a 632 nm He-Ne laser as a reference laser by make them coaxial at the starting point. The internal structure of the component is shown in Fig. 2. It consists of CO_2 laser, He-Ne laser, 25 × beam expander (for 10.6 μm), 20 × beam expander (for 633 nm), 1/2 wave plate and its electric regulator, a plane mirror and a beam combiner; the 1/2 wave plate is used to adjust the polarization angle of the CO_2 laser. The beam combiner is a coated dichroic mirror with ZnSe substrate. Its transmittance of 10.6 μm wavelength can reach 99.1% (theoretical value, actual measured value is 97.4% when laser output power is set to 137 W), and the reflectivity of 632 nm wavelength can reach more than 90%. These components are integrated on one optical platform to reduce the influence of external vibration.

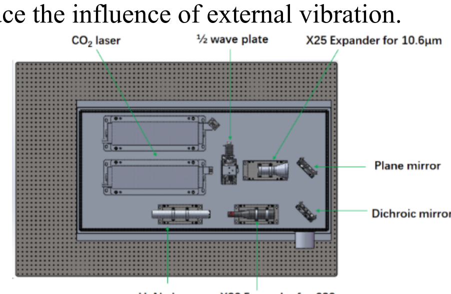

Figure 2: Laser combination module's layout.

If the two lasers are coaxial well, the transmission direction and focus position of the CO_2 laser can be "visualized" by the reference laser. This provides a basis for the installation and optical path feedback correction of the entire laser system.

ISBN: 978-3-95450-214-1 ISSN: 2673-5490 doi:10.18429/JACoW-IPAC2021-THPAB063

Adjustment Module

The function of this module is to adjust the laser direction and its axis position. Each mirror box and lens can be adjusted manually. there is one mirror frame adjusted by 3 piezoelectric drivers in mirror box #4 and #5 respectively, as shown in Fig. 3. Both can be controlled remotely to compensate the deviation caused by temperature drift or low-frequency vibration, and thus maintain the stability of the laser transmission direction. The turntable in mirror box #4 play the role of switching the optical path between two operation modes.

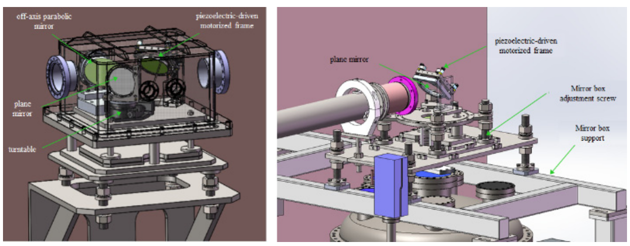

Figure 3: Piezoelectric-driven motorized frame in mirror box #4 (left) and #5 (right).

The main adjustment parameters of the piezoelectric-driven motorized frame are listed in Table 1. Although the typical single step length of the piezoelectric frame is 30 nm, the actually measured angle resolution is 1.5 µrad, which is about 2 times of the designed parameter.

Table 1: Designed Adjustment Parameters of the Piezoelectric-Driven Motorized Frame

Parameter	Range	Resolution
Z	$\pm$5 mm	0.03 µm
Roll(r-x)	$\pm 2.5^{\circ}$	0.15”
Roll(r-y)	$\pm 2.5^{\circ}$	0.15”

Detection Module

The detection module includes coaxial detector of CO_2 laser and He-Ne laser, and direction detectors of laser. The former is mainly used to check the coaxiality of the combined beam periodically, and the latter can be used with the adjustment module to realize the feedback adjustment of the laser direction.

Coaxial detector, shown in Fig. 4, is installed near the point where the focal points of off-axis parabolic mirrors coincide. When detection starts, the infrared imaging card is moved in to block light by a translation stage.

Turn on the CO_2 laser and He-Ne laser separately, take pictures of the spots on the card, fit and compare the center position parameters of the two spot, the coaxiality of the CO_2 laser and the He-Ne laser would be obtained. The repetitive positioning accuracy of the card is 2 µm, and the repetitive attitude accuracy is 10”. The camera resolution of the picture is 20 µm and the focal length of the off-axis parabolic mirror is 5.4 m, So the Coaxial detector can detect angle difference no less than 4 µrad. The measured coaxiality result is smaller than 8 µrad.

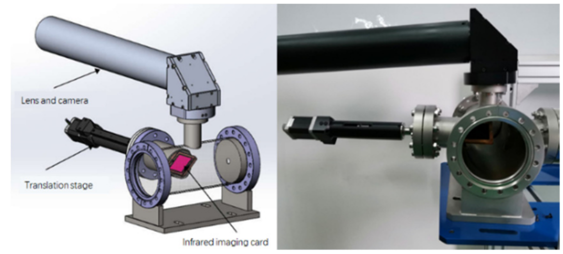

Figure 4: Coaxial detector’s model (left) and photo (right).

For laser pointing detection, a dichroic mirror is used to reflect the He-Ne laser out of the main optical path and irradiate it to the detector through the focusing mirror, shown in Fig. 5. The pixel size of the detector is 4.5 µm, the center peak fitting accuracy is 2 pixel, and the focal length of the visible light focusing lens is 3 meters, so the corresponding detection accuracy is 5 µrad.

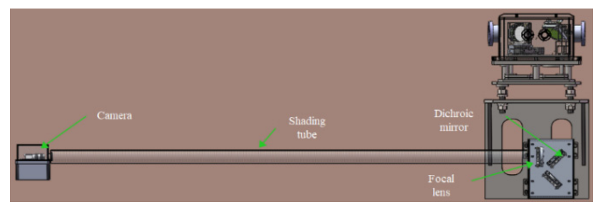

Figure 5: Direction detectors of laser’s layout under mirror box #4.

Control Module

The control module allows the previous modules to work together to achieve several useful features:

1. Feedback stability: adjust the piezoelectric-driven motorized frame to let the spot on the direction detector stay within 2 pixels of the starting point will realize a feedback system. Once established, the PV value of laser pointing direction’s jitter will be reduced to 5 µrad, make the pointing much more stable.
2. Automatic scanning: which will give a map of intensity of the gamma ray at each angle if the gamma intensity is feedback. The optimal direction of laser with strongest gamma intensity can be found this way.

The control module also has some built-in interlocking functions, e.g. when the coaxial detection is turned on, the CO_2 laser’s power is limited to a fixed small value to avoid the damage of the infrared imaging card. Whenever the He-Ne spot is not visible on the direction detector, the CO_2 laser will be turned off.

POINTING STABILITY

As mentioned in the introduction part, one of the most important parameter of the laser transport system is the pointing stability. So we studied it theoretically during design phase and measured it after the installation.

Theoretical Calculation

The pointing stability of the entire system are mainly limited by the following factors:

ISBN: 978-3-95450-214-1 ISSN: 2673-5490 doi:10.18429/JACoW-IPAC2021-THPAB063

- Laser output beam's pointing stability.
- System vibration.
- The influence of the optical window on the light path.

The angle stability of the CO_2 laser is less than 250 μrad according to the manual, and will be reduced to no more than 10 μrad after the 25 times expansion.

According to the results of environmental vibration detection, the vibration amplitude inside the entire storage ring is within 1 μm in the frequency range of 1-100 Hz, typically the amplitude of the XBPM on the optical transmission system is within 0.5 μm, while the XBPM height is about 1.2 meters, the corresponding angle change is 0.4 μrad.

Simulation shows that the eigenfrequency the support frames are nearly all larger than 100 Hz. The harmonic response simulation results in Fig. 6 show that if the displacement excitation of 350 nm is set in the vertical direction, with 250 nm in the east-west direction, and 220 nm in the north-south direction, the maximum deformation does not exceed 2.8 μm, and the influence on the beam pointing is below 0.28 μrad.

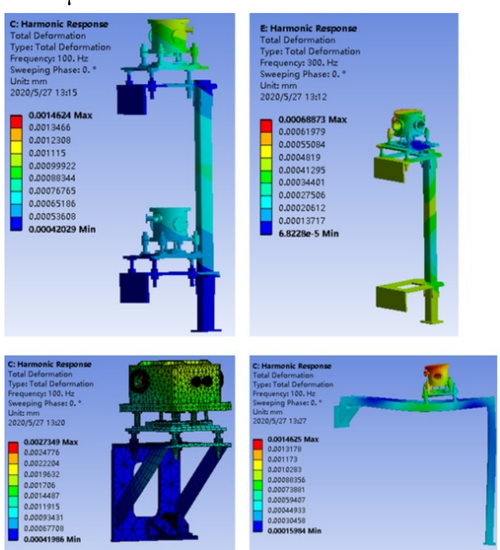

Figure 6: Harmonic response simulation results of the mirror box #1, #2 (upleft), #3 (upright), #4 (downleft), #5 (downright) with their support.

The thickness of the ZnSe window is about 5 mm. Assuming that the incident light enters the flange at an angle of 1º, then the deviation between He-Ne laser and CO_2 laser is 2 μm, which has little effect on the overall pointing accuracy.

In summary, the point stability is below 10 μrad and could be detected through reference He-Ne laser.

Experimental Measurement

In fact, thermal deformation from laser absorption or environment temperature change, and airflow in connection parts can also influence the pointing stability, which is hard to calculate accurately. So we measured the jitter of He-Ne laser when CO_2 laser is on with max output power in 10 min with 10 Hz sample rate in two operation mode (see Figs. 7 and 8).

The results in Table 2 show that the RMS value of jitter is about 7 μrad, consistent with theoretical calculation.

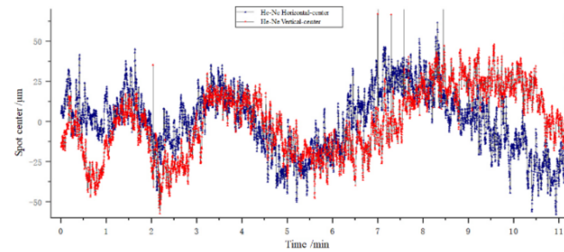

Figure 7: The jitter of the fitting results of He-Ne spot's center before entering multi-pass chamber.

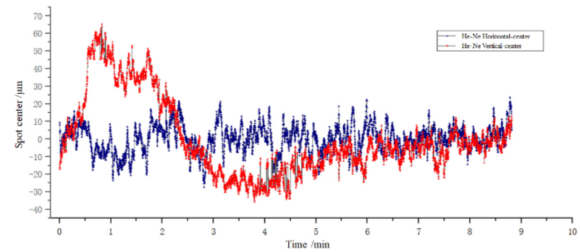

Figure 8: The jitter of the fitting results of He-Ne spot's center before entering interaction chamber.

Table 2: Jitter of the Direction

Column 1	Length RMS [μm]	Angle RMS [μrad]
B mode H-deviation	19.3	6.44
B mode V-deviation	20.5	6.82
S mode H-deviation	7.70	2.57
S mode V-deviation	21.6	7.19

CONCLUSION

The laser power is decreased during the transportation, so the transmission efficiencies of CO_2 laser at 10.6 μm are measured, as in Table 3. The laser source output power measured is 137 watts.

Table 3: Transmission Efficiencies

Mode	Position	Power [W]	Efficiency [%]
Backscattering	Before multi-pass chamber	95.8	70.0
Slanting	Before interaction chamber	96.8	70.6

In conclusion, the laser transport system can realize spot monitoring and feedback control, and automatically correct the transmission light path, accomplish the coaxial transmission of 632 nm reference laser and CO_2 laser with coaxiality less than 8 μrad and pointing jitter at about 7 μrad, under two operation modes. The total transmission efficiency is about 70%.

More test including the measurement of waist size can be performed in the future.

ISBN: 978-3-95450-214-1 ISSN: 2673-5490 doi:10.18429/JACoW-IPAC2021-THPAB063

REFERENCES

[1] W. Guo *et al.*, "A high intensity beam line of γ-rays up to 22 MeV energy based on Compton backscattering", *Nucl. Instrum. Methods A*, vol. 578, no. 3, pp. 457-462, 2007. doi:10.1016/j.nima.2007.05.322

[2] H. Xu *et al.*, "Interaction Chamber Design for an Energy Continuously Tunable Sub-MeV Laser-Compton Gamma-Ray Source", *IEEE Trans. Nucl. Sci.,* vol. 63, no. 2, pp. 906-912, 2016. doi:10.1109/TNS.2015.2496256